


Learning Quantized Adaptive Conditions for Diffusion Models

Yuchen Liang¹ , Yuchuan Tian², Lei Yu³, Huaao Tang³, Jie Hu³, Xiangzhong Fang¹, and Hanting Chen³

¹ School of Mathematical Sciences, Peking University

² State Key Lab of General AI, School of Intelligence Science and Technology, Peking University

³ Huawei Noah's Ark Lab

ycliang@pku.edu.cn, chenhanting@huawei.com

Abstract. The curvature of ODE trajectories in diffusion models hinders their ability to generate high-quality images in a few number of function evaluations (NFE). In this paper, we propose a novel and effective approach to reduce trajectory curvature by utilizing adaptive conditions. By employing an extremely light-weight quantized encoder, our method incurs only an additional 1% of training parameters, eliminates the need for extra regularization terms, yet achieves significantly better sample quality. Our approach accelerates ODE sampling while preserving the downstream task image editing capabilities of SDE techniques. Extensive experiments verify that our method can generate high quality results under extremely limited sampling costs. With only 6 NFE, we achieve 5.14 FID on CIFAR-10, 6.91 FID on FFHQ 64×64 and 3.10 FID on AFHQv2.

Keywords: Accelerated Sampling · Diffusion Models · Generative Modeling · Visual Tokenization

1 Introduction

Generative models based on ordinary differential equations (ODEs) have led to unprecedented success in various domains, including image synthesis [9], audio synthesis [16], 3D reconstruction [31], and video generation [10]. These models transform a tractable noise distribution to the data distribution with differentiable trajectories to Early attempts faced limitations due to the requirement of simulating ODEs, which hindered their practical applicability. Recent advancements in score-based diffusion models [5, 8, 37, 38] avoid explicit ODE generation by employing a forward stochastic differential equation (SDE) process with an accompanying Probability Flow (PF) ODE. By numerically simulating the PF-ODE, diffusion models enable the generation of high-quality samples. This process requires multiple evaluations of a neural network leading to slow sampling speed.

Efforts have been made to accelerate the sampling process and fall into two main streams. One stream aims to build a one-to-one mapping between the data

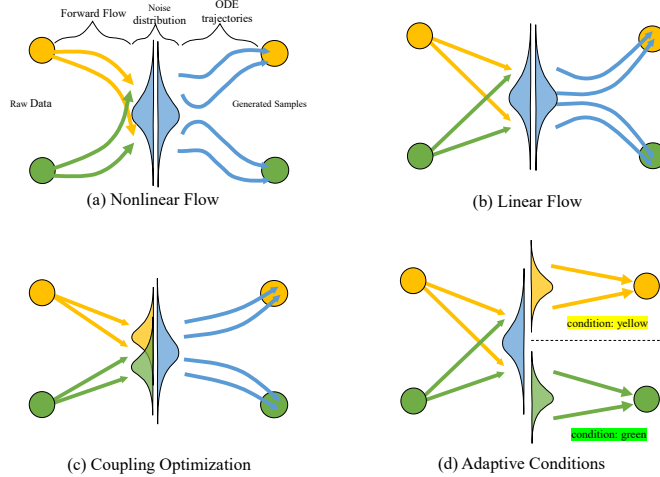


Fig. 1: (a) Denoising diffusion models with nonlinear forward flow [8, 38] have complex ODE trajectories. (b) Linear Flow models [12, 22, 29, 35] still have highly curved ODE trajectories. (c) Coupling optimization [19] methods try to reduce curvature by trajectory relocation, but are limited by the difficulty of keeping the noise distribution unchanged. (d) Adaptive Conditions untie the crossover between forward trajectories without compromising the full simulation accuracy.

distribution and the pre-specified noise distribution [2, 22, 25, 32, 36], based on the idea of knowledge distillation. However, these methods require huge efforts on training. Training such a student model should carefully design the training details and takes a large amount of time to train the model (usually several GPU days). Moreover, as distillation-based models directly build the mapping like typical generative models, they suffer from the inability of interpolating between two disconnected modes [33]. Therefore, distillation-based methods may fail in some downstream tasks requiring such an interpolation. Besides, distillation-based models cannot guarantee the increase of sample quality given more NFE and they have difficulty in likelihood evaluation. The other stream of methods focuses on designing faster numerical solvers to increase step size while maintaining the sampling quality [6, 12, 21, 23, 35, 44, 45]. Although these methods have successfully reduced the number of function evaluations (NFE) from 1000 to less than 20, almost without affecting the sample quality. Nevertheless, these methods still face the challenge of the intrinsic truncation errors rooted in the curvature of the trajectory. The sampling quality deteriorates sharply when the sampling budget is further limited.

In order to reduce the trajectory curvature, Rectified Flow [22] provides a different understanding of diffusion models from the transport mapping perspective. The PF-ODE can be considered as the result of a rectification process, which unties the predefined forward coupling flows. In the case of score-based

methods, independent coupling is utilized, which can be seen as a special case in the theory of Rectified Flow. These PF-ODE trajectories will be curved to avoid crossing. From this viewpoint, there are two key points to reduce the curvature of PF-ODE trajectories: the first is to use linear forward flow [12, 20, 35], and the second is to reduce the intersection of the forward trajectory to maintain straightness. Previous research aimed to reduce the intersection by optimizing coupling [19, 30] via trajectory relocation. However, the optimization process is challenging to maintain the marginal noise distribution. And a series of stochastic sampling [23, 42] and part of distillation techniques [26, 43] designed for the score-based model are no longer available, which hinders the acceleration of the simulation process and impedes the applicability of these methods.

In this paper, we propose a novel and effective approach for reducing the intersection. At the same time, the key properties of score-based models is retained. Our approach is motivated by a straightforward analogy: when there is a large number of pedestrians needing to cross a road from both sides, city authorities would consider installing traffic lights instead of moving the road. Similarly, we lead the backward process with adaptively learned quantized conditions, which allows the backward PF-ODE trajectories to pass through intersection areas without the need for significant curvature or trajectory relocation. A schematic diagram is shown in Fig. 1. Our contribution can be summarized as follows:

- We investigate the relationship between the degree of forward flow intersection and the quality of the few-step sampling. We provide theoretical support for the positive correlation of the intersection and the quality of the few-step sampling.
- We present a plug-and-play approach with a quite small additional training cost to reduce the degree of intersection, which is the first method that does not require trajectory relocation and additional regularization.
- We conduct extensive comparison and ablation experiments on the CIFAR-10, MNIST, FFHQ and AFHQv2 to verify that our method can achieve superior performance compared to the original diffusion models in both few-step sampling and full sampling generation.

2 Background

2.1 Diffusion Model

Diffusion models set a stochastic differential equation (SDE) [38]

$$dx_t = \mu(x_t, t)dt + \sigma(t)dw_t \quad (1)$$

where $t \in [0, T]$, $T > 0$ is a fixed positive constant, w_t is the standard Wiener process and $\mu(\cdot, \cdot)$ and $\sigma(\cdot)$ are the drift and diffusion coefficients respectively. We denote the distribution of x_t as $p_t(x)$ and set $p_0(x)$ as the data distribution. A remarkable property of this SDE is Remarkably, there exists a probability flow ODE

$$dx_t = [\mu(x_t, t) - \frac{1}{2}\sigma(t)^2\nabla_x \log p_t(x)]dt \quad (2)$$

sharing the same marginals with the reverse SDE [27]. To simulate the PF-ODE, a U-Net $s_\theta(x, t)$ is usually trained to estimate the intractable score function $\nabla_x \log p_t(x)$ via score matching [11, 41]. The SDE in Eq. (1) is designed such that p_T is close to a tractable Gaussian distribution $\pi(x)$. During sampling stage, we will sample a noise image from $\pi(x)$ to initialize the empirical PF ODE and solve it backwards in time with any numerical ODE solver.

2.2 Rectified Flow

From the view of transport mapping, Rectified Flow [22] offers an alternative perspective which is fully explained under the ODE scheme. Let $\mathbf{X} = \{X_t : t \in [0, T]\}$ be any time-differentiable forward flow process that couples the data $X_0 \sim p_{data}$ and the noise $X_T \sim p_{noise}$. Let \dot{X}_t be the time derivative of X_t . The rectified flow induced from \mathbf{X} is defined as

$$dZ_t = v^{\mathbf{X}}(Z_t, t), \text{ with } Z_T = X_T \quad (3)$$

where $v^{\mathbf{X}}(z, t) = \mathbb{E}[\dot{X}_t | X_t = z]$. And $v^{\mathbf{X}}$ can be estimated by minimizing the conditional flow matching (CFM) objective

$$L_{\text{CFM}}(\theta) := \int_0^T w_t \mathbb{E} \|\dot{X}_t - v_\theta(X_t, t)\|^2 dt, \quad (4)$$

where $w_t : (0, T) \rightarrow (0, +\infty)$ is a positive weighting sequence. The marginal preserving property [22], $Law(Z_t) = Law(X_t) \quad \forall t \in [0, T]$, ensures that we can generate samples by simulating the reversed ODE from tractable random variable X_T . With independent coupling (X_0, X_T) , different forward process correspond to different diffusion models:

Nonlinear Flows

$$\text{VP [8]} : X_t = \alpha(t)X_0 + \sqrt{1 - \alpha(t)^2}X_1, X_1 \sim \mathcal{N}(0, I) \quad (5)$$

$$\text{VE [38]} : X_t = X_0 + \sqrt{t}\xi, X_T \approx \sqrt{T}\xi \sim \mathcal{N}(0, TI) \quad (6)$$

Linear Flows

$$\text{EDM/DDIM [12, 35]} : X_t = X_0 + t\xi, X_T \approx T\xi \sim \mathcal{N}(0, T^2I), \quad (7)$$

$$\text{RectifiedFlow [22]} : X_t = (1 - t)X_0 + tX_1, X_1 \sim \mathcal{N}(0, I). \quad (8)$$

Compared with nonlinear flow methods, linear flows have showed a significant effect on sampling acceleration.

2.3 Coupling Optimization

In order to further reduce the cost of ODE trajectory simulation, Liu etc. [22] introduce an multistage optimization approach where the original coupling

(X_0, X_1) is substituted with rectified coupling (Z_0, Z_1) . Lee etc. [19] and Pooladian etc. [30] adopt joint training to avoid additional training iterations and to prevent errors caused by ODE simulation. The joint training relies on the following bias-variance decomposition of the CFM loss:

$$L_{CFM} = L_{FM} + V((X_0, X_1)) \quad (9)$$

where

$$L_{FM} := \int_0^T w_t \mathbb{E} \|\mathbb{E}[\dot{X}_t | X_t] - v_\theta(X_t, t)\|^2 dt \quad (10)$$

judges the accuracy of direction fitting and

$$V((X_0, X_1)) := \int_0^T w_t \mathbb{E} \|\dot{X}_t - \mathbb{E}[\dot{X}_t | X_t]\|^2 dt \quad (11)$$

measures the intersection of forward flow.

When $V((X_0, X_1))$ approaches zero, the curvature of rectified trajectories also tends to zero. Therefore, the coupling optimization can be performed jointly with direction fitting by minimizing L_{CFM} without the need for simulation of ODE trajectories.

However, it is challenging to maintain the marginal distribution for X_0 and X_1 . Multisample flow matching [30] constructs a doubly-stochastic matrix for the coupling distribution, which limits by the batch size. And in the work [19] of Lee etc., they employ a reparamized noise encoder, which compromises to the error between the encoded distribution and the prior distribution. To address this challenge, we propose an alternative approach to reduce the intersection of the forward flow.

3 Adaptive Conditions

We discriminate the forward trajectories with different adaptive conditions represented by Y , which can be considered as pseudo-labeling of the image data X_0 and independent of the noise X_1 . The allocation of conditions is carried out by an autoencoder $q_\phi(x_0, y) = p_{data}(x_0)q_\phi(y|x_0)$ and led by the conditional CFM loss

$$L_{CFM} = \int_0^T w_t \mathbb{E}_{X_0, Y \sim q_\phi} \|\dot{X}_t - v_\theta(X_t, t, Y)\|^2 dt, \quad (12)$$

which is an expectation of unconditional L_{CFM} with different conditions Y .

3.1 Discretization Error Control

We present theoretical evidence demonstrating that for linear flows L_{CFM} can effectively control the influence of discretization error accumulation on the generation quality and address the inconsistencies that impact distillation efficiency.

Theorem 1. Let $S_{t,y} \sim \tilde{p}_t$ be a simulation of $X_t|_{Y=y} \sim p_{t,y}$ and

$$S_{t,y} - \Delta t v_\theta(S_{t,y}, t, y) =: d_{t,\Delta t}(S_{t,y}, y) \sim \tilde{p}_{t-\Delta t,y}, \quad (13)$$

be the one-step further simulation of $X_{t-\Delta t,y} \sim p_{t-\Delta t,y}$. And $d_{t,\Delta t}(S_{t,Y}, Y) \sim \tilde{p}_{t-\Delta t}$ denote the overall simulation of $X_{t-\Delta t} \sim p_{t-\Delta t}$. Then we can control the Wasserstein distance

$$W(\tilde{p}_{t-\Delta t}, p_{t-\Delta t}) \leq [\mathbb{E}_Y W^2(\tilde{p}_{t-\Delta t,Y}, p_{t-\Delta t,Y})]^{1/2} \quad (14)$$

$$\leq \Delta t \cdot l_{CFM}(t) + L[\mathbb{E}_Y W^2(\tilde{p}_{t,Y}, p_{t,Y})]^{1/2} \quad (15)$$

where L is the Lipschitz constant for $d_{t,\Delta t}(\cdot, y)$ and

$$l_{CFM}(t) = [\mathbb{E}\|\dot{X}_t - v_\theta(X_t, t, Y)\|^2]^{1/2} \quad (16)$$

is a component of the optimization objective defined in Eq. (12)

$$L_{CFM} = \int_0^T w_t [l_{CFM}(t)]^2 dt. \quad (17)$$

Proof. The proof parallels the proof of the Wasserstein distance upper bound for score-based generative models [18]. A tighter upper bound can also be obtained following the technique provided by [18]. We provide a complete proof in supplementary materials.

And for unconditional L_{CFM} there is a more intuitive and concise version of Eq. (15).

$$W(\tilde{p}_{t-\Delta t}, p_{t-\Delta t}) \leq \underbrace{\Delta t}_{\text{step size}} \cdot \underbrace{l_{CFM}(t)}_{\text{new error}} + \underbrace{L}_{\text{amplifying coefficient}} \cdot \underbrace{W(\tilde{p}_t, p_t)}_{\text{original error}} \quad (18)$$

Theorem 1 have shown that a smaller loss L_{CFM} can provide quality assurance for single-step update with Euler solver, and more advanced deterministic and stochastic solvers can be regarded as corrections based on this result. Specifically when setting $\Delta t = t$ the theorem shows that the gap between the predicted image distribution and the groundtruth distribution can be bounded by L_{CFM} . The experiments of [19] and [34] showed that a smaller L_{CFM} can improve the efficiency and final performance of distillation. [30] also clarified that L_{CFM} can reduce the variance of stochastic gradients, which provides a more stable training process and convergence speed. For the score-base diffusion model, L_{CFM} cannot be optimized to zero because of the intersection of forward flows. Fortunately, as shown in Tab. 1, coupling optimization and adaptive condition provide more optimization space and when the L_{CFM} approaches zero, the ode trajectory tends to be completely straight.

Table 1: The result of the optimized L_{CFM} and average curvature of ODE trajectories after training by 15M images drawn from the dataset Cifar10. We use the same model configs and sampler as Reparamized Noise Encoder(RNE) [19] with a prior regularization $\beta = 20$ for a fair comparison.

Method	$L_{CFM} \downarrow$	Curvature \downarrow	FID \downarrow	
			Heun w/5 NFE	RK45
RectifiedFlow	0.176	0.46	37.19	2.66
RNE	0.153	0.38	24.54	2.45
Adaptive Condition	0.132	0.40	19.68	2.43

3.2 Quantized Condition Encoder

For learning the adaptive conditions, we have the flexibility to use any variational autoencoder (VAE) [15]. However, unlike reparamized noise encoder [19], the condition coding space is decoupled from the noise space. This decoupling provides more freedom in choosing the encoding strategy. We chose to use a quantized encoder because it doesn't suffer from posterior collapse, which is a common issue in other VAEs. A quantized encoder with a sufficiently large coding space can handle high-resolution image reconstruction effectively.

Typically, a visual tokenization generative model [7,40] requires an additional sequence model to learn the distribution of the quantized feature map. To avoid introducing extra training and inference costs, we use a single quantized vector instead of a quantized feature map. This significantly reduces the coding space dimensionality by several orders of magnitude. However, it also allows us to use a lightweight encoder(smaller than 0.8M), and the empirical distribution of the code vectors can be easily collected online.

We first encode the image x into a d -dimensional vector $y = E_\phi(x)$ via a neural network encoder, and then discretize it using a finite scalar quantization [28] with some minor modifications. For each channel y_i , we use a function f to restrict its output to L discrete integers. We choose f to be $f : y \mapsto \lfloor L \cdot \sigma(y) \rfloor$ where $\sigma(y) = 1/(1 + e^{-y})$ is the sigmoid function, which is more symmetric compared to the original version $round(\lfloor L/2 \rfloor \tanh(y))$ when L is even. As a result, the value space of $y_q = f(y)$ forms an implied codebook $C = \{0, 1, \dots, L - 1\}^d$, which is given by the product of these per-channel codebook sets, with $|C| = L^d$. Finally, we use the Straight-Through Estimator [1] to copy the gradients from the decoder input to the encoder output, which allows us to obtain gradients for the encoder. This can be implemented easily using the "stop gradient" (sg) operation as follows: $f_{STE} : y \mapsto y + sg(f(y) - y)$.

Each condition code $y_q \in C$ corresponds to a data slice, which can be viewed as a form of pseudo-labeling. We train diffusion models with quantized condition encoder just as in a conditional manner. We use two MLP layers to map the condition code to the same dimension as the time embedding and then add them together. Then, we input the combined embedding and noised image into the decoder. A visual schematic of our approach is shown in Figure 2.

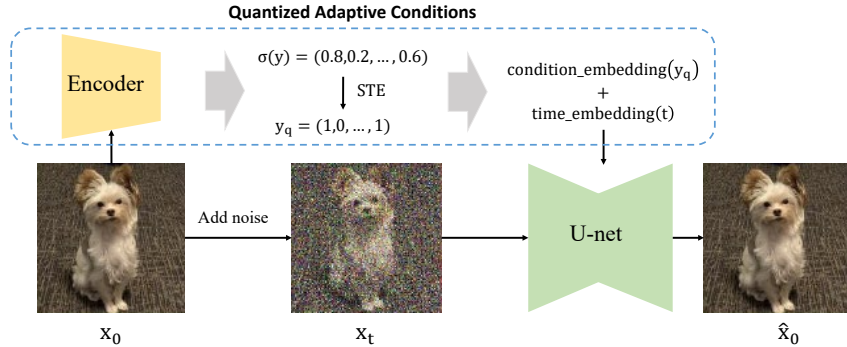


Fig. 2: A visual schematic of our approach.

3.3 Online Sampling Weight Collection

Diffusion models, even when they converge, still have non-zero gradients. Therefore, exponential moving average (EMA) is often used to update the parameters more stably. However, this introduces a time inconsistency problem between the parameters and the condition sampling weight. To deal with this problem, we propose two sampling weight collection strategies:

- **Offline collection:** Also update the condition encoder with EMA and then collect the sampling weight for the training dataset with the final checkpoint of the EMA encoder.
- **Online collection:** Inspired by EMA normalization [3], we use EMA synchronized with the model parameters to update the sampling weight for each mini-batch during the training process.

As shown in Tab. 2, the online sampling weight exhibits significantly better performance on both few step generation with Heun’s method and full simulation generation with an adaptive step solver RK45.

Table 2: A comparison of online and offline collection, based on ODE trajectory of RectifiedFlow with a condition codebook size 2^{20}

Collection Strategy	FID↓		
	Heun w/ 5 NFE	Heun w/ 7 NFE	RK45
Offline	21.07	14.40	5.96
Online	19.68	13.22	2.61

3.4 Training and Sampling

We train the condition encoder and image denoiser networks jointly. Following previous works, we update the model parameters and the online sampling weights with EMA. The complete training process of quantized adaptive conditions can be summarized as Algorithm 1.

Algorithm 1 Quantized Adaptive Conditions Training

Require: dataset \mathcal{D} , noise level distribution p_σ , encoder initial parameter ϕ , denoiser initial parameter θ , loss weighting $\lambda(\cdot)$, learning rate η , EMA decay rate μ

- 1: $\theta^- = \theta$ ▷ Copy initial parameter to EMA model
- 2: $w \leftarrow 0_{1 \times |c|}$ ▷ initiate sampling weight with zeros
- 3: **repeat**
- 4: Sample $x \sim \mathcal{D}$, $t \sim p_\sigma$ and $z \sim \mathcal{N}(0, I)$
- 5: $y \leftarrow E_\phi(x)$
- 6: $y_q \leftarrow y + \text{sg}([L \cdot \sigma(y)] - y)$ ▷ Compute condition codes by STE
- 7: $x_t \leftarrow x + tz$
- 8: $\mathcal{L}(\theta, \phi) \leftarrow \lambda(t) \|x - D_\theta(x_t, t, y_q)\|^2$
- 9: $\theta \leftarrow \theta - \eta \frac{\partial \mathcal{L}}{\partial \theta}$, $\phi \leftarrow \theta - \eta \frac{\partial \mathcal{L}}{\partial \phi}$
- 10: $\theta^- \leftarrow \mu \theta^- + (1 - \mu) \theta$
- 11: $w_{batch} \leftarrow \text{Count}(\text{Index}(y_q))$ ▷ Collect batch sampling weights of code indices
- 12: $w \leftarrow \mu w + (1 - \mu) w_{batch}$ ▷ Update sampling weights by EMA
- 13: **until** convergence
- 14: **return** θ^-, w

During the sampling stage, we also follow a procedure that is similar to regular conditional diffusion models. Here is a breakdown of the steps:

1. Code Index Selection: Randomly select an condition index based on the collected sampling weights. This index corresponds to a specific condition code.
2. Noise Sampling: Sample a random noise from the distribution of X_T or an approximation of it. This sampled noise serves as the initial point for the reverse ODE or SDE process.
3. Score Function Estimation: Utilize the denoiser’s output to compute an estimation of the score function conditioned on the selected condition code. This estimation helps guide the sampling process.
4. Reverse Process Simulation: Use a deterministic or stochastic solver to numerically simulate the reverse process. This solver propagates the initial point backward in time, following the dynamics defined by the reverse ODE or SDE. The result is a generated sample that incorporates the selected condition code and the sampled noise.

By incorporating adaptive conditions, the reverse process simulation ensures that the generated samples follow the desired dynamics defined by the reverse ODE or SDE.

Table 3: FIDs with different settings of condition encoder.

Dataset	CIFAR-10	MNIST	
Solver	Heun	Euler	
NFE	9	4	16
w/o condition	12.92	31.67	11.16
VAE(optimal weight)	12.23	10.75	5.63
FSQ($L = 8, d = 4$)	11.07	8.50	1.81
FSQ($L = 4, d = 6$)	10.85	7.49	1.71
FSQ($L = 2, d = 12$)	10.83	6.36	1.19

Table 4: FID on CIFAR10 with Heun’s method when scaling the codebook size

Codebook size\NFE	5	7	9
w/o a codebook	37.19	18.60	12.92
$ \mathcal{C} = 2^{12}$	21.86	13.78	10.83
$ \mathcal{C} = 2^{14}$	21.38	13.74	10.71
$ \mathcal{C} = 2^{16}$	20.18	13.22	10.60
$ \mathcal{C} = 2^{18}$	20.13	13.17	10.34
$ \mathcal{C} = 2^{20}$	19.68	13.11	10.28

4 Experiments

4.1 Quantized Condition Encoder

Table 3 demonstrates the improvement of generated image quality achieved by different condition encoders. We use Rectified Flow [22] as the baseline and adopt the same training configuration and sampling procedure temporarily in this subsection for a fair comparison. Following RNE [19], we choose the encoder network with $\frac{1}{4}$ channels and $\frac{1}{2}$ blocks of the counterpart U-net network. And it’s worth mentioning that we only need the encoder part of the U-net network, so we used even fewer extra parameters than RNE [19]. Regardless of the type of condition encoders used, quantized adaptive conditions can consistently enhance the few-step generation performance. The Finite Scalar Quantizations (FSQ) excels in avoiding prior collapse and outperforms vanilla VAE significantly.

For a fixed codebook size of 2^{12} , smaller levels yield better performance. This is because the quantized code forms an information bottleneck for image reconstruction, and smaller levels provide more dimensions to capture essential details. Therefore, we set the level $L = 2$ to obtain a higher-quality representation of the images during the generation process.

As shown in Tab. 4, scaling the codebook size can always demonstrate better generation quality. Even when the codebook size reaches 2^{20} , which exceeds the number of training samples by far, the sampling weights as a model buffer only occupy a parameter count of 1M.

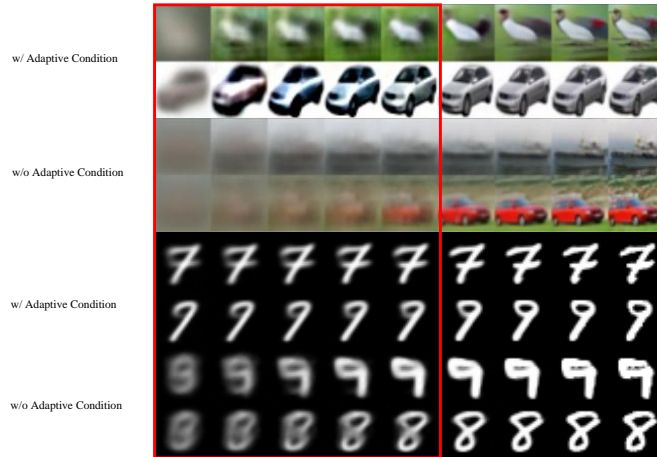


Fig. 3: Visualization of intermediate samples. Adaptive conditions allow for sharper initial predictions at high noise level, as indicated by red boxes.

4.2 Working with Reparamized Noise Encoder

Since the code space of condition is independent of the noise space, the quantized condition encoder can be applied with the reparamized noise encoder together to further reduce the curvature. These two approaches can cooperate efficiently with each other by sharing the encoder network backbone. As shown in Tab. 5, the best results are obtained by using both methods.

Table 5: Applying reparamized noise encoder (RNE) and quantized adaptive conditions (QAC) at the same time.

NFE	5	7	9
RectifiedFlow	37.19	18.60	12.92
w/ RNE only	24.54	13.99	10.21
w/ QAC only	19.68	13.11	10.28
w/ RNE & QAC	18.20	12.11	9.58

4.3 Comparison with state-of-the-arts

Table 7 shows the unconditional synthesis results of our approach on real-world image datasets including CIFAR-10 [17] at 32×32 resolution, FFHQ [13] and AFHQv2 [4] at 64×64 resolution. Considered as a one-session training approach, in Tab. 6 we compare our method with other one-session training methods including a variety of diffusion models such as NCSN++, DDPM, EDM, Rectified Flow and RNE and the accelerated sampling techniques. We train quantized adaptive

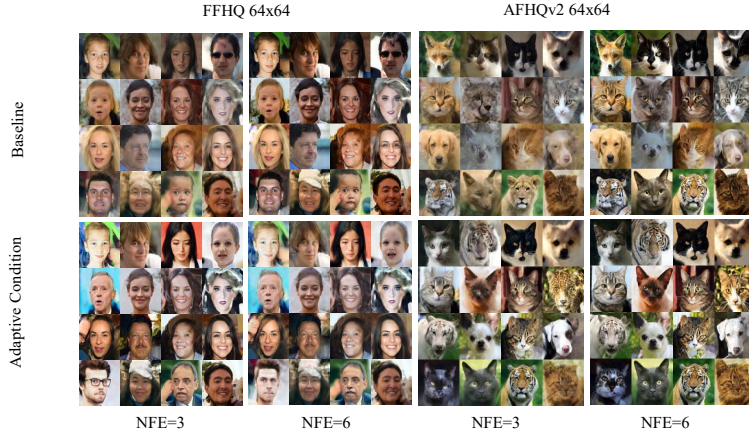


Fig. 4: Qualitative comparison between our method and baseline on CIFAR-10, FFHQ and AFHQv2.

Table 6: Performance comparisons on CIFAR-10.

Model	NFE↓	FID↓
Diffusion Models		
DDPM [8]	1000	3.17
NCSN++ [35]	2000	2.20
VDM [14]	1000	7.41
LSGM [39]	147	2.10
RectifiedFlow [22]	127	2.58
EDM [12]	35	2.01
RNE [19]	9	8.66
Accelerated Sampler		
DDIM [35]	10	15.69
DPM-solver [23]	8	10.30
DPM-solver++ [24]	6	11.85
UniPC [45]	6	11.10
DEIS [44]	6	9.40
DPM-Solver-v3 [46]	6	8.56
AMED [47]	6	6.63
QAC(Ours)	20	2.10
QAC(Ours)	6	5.14

conditions with a codebook size 2^{20} under the same training configuration as EDM [12] and adopt accelerated sampler iPNDM [44] with the polynomial time schedule [12] and analytical first step [6]. See the supplementary materials for details about the training configuration and sampling process. In the Tab. 7, we

Table 7: Sampling from Quantized Adaptive Conditions(QAC) with iPNDM(afs).

NFE	3	4	5	6
CIFAR10-32x32				
EDM [12]	26.21	14.43	8.17	5.32
QAC	21.06	12.48	7.50	5.14
FFHQ-64x64				
EDM [12]	27.94	19.90	13.30	8.50
QAC	22.92	15.34	9.42	6.91
AFHQv2-64x64				
EDM [12]	15.60	8.58	5.55	3.78
QAC	8.32	5.04	3.51	3.10

Algorithm 2 Zero-Shot Image Editing

Require: Denoising model D , condition code encoder E , time steps $\{t_n\}$, reference image z

- 1: $z \leftarrow A^{-1}[(Az) \odot (1 - \Omega) + 0 \odot \Omega]$
- 2: $x \leftarrow z$
- 3: **for** $t = t_1$ to t_N **do**
- 4: $y \leftarrow E(x)$
- 5: Sample $x \sim \mathcal{N}(x, t^2 \mathbf{I})$
- 6: $x \leftarrow D(x, t, y)$
- 7: $x \leftarrow A^{-1}[(Az) \odot (1 - \Omega) + (Ax) \odot \Omega]$
- 8: **end for**
- 9: **return** x

can see that the performance gap between our method and the baseline is huge when the sampling budget is limited. For instance, our method achieved an FID score of 8.32 on AFHQv2, which is significantly better than the baseline’s score of 15.60 when NFE is 3. Our method exhibits superior sample qualities across all NFE, even in the case of full sampling. See Fig. 4 for visual comparison. Additional qualitative results are provided in supplementary materials.

4.4 Zero-Shot Image Editing

Comparing with coupling operation, adaptive conditions does not affect the use of SDE-based technologies such as SDEidt. Note that

$$p(x_{t_{n+1}}|x_{t_n}) = p(x_{t_{n+1}}|x_{t_n}, y)p(y|x_0)p(x_0|x_{t_n}).$$

According to the Algorithm 2, shown in Fig. 5, our method is competent for various image editing tasks such as super-resolution, colorization and inpainting.

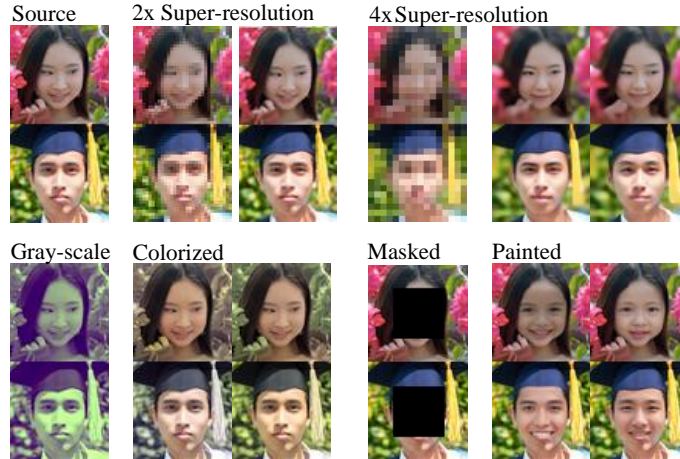


Fig. 5: Our method allows SDE-based zero-shot image editing applications such as super-resolution, colorization and inpainting. In the experiments, we used Karras’s schedule with steps $N = 40$.

5 Discussion and Limitations

One limitation is that for our encoding space, we use a code vector as adaptive condition for practical conveniences: sampling is easily implemented and the code sampling weight can conveniently be collected. However, we can not fully reconstruct the image in one step from such a short binary vector. To further enhance the expressive power of the encoder, we believe that a feature map can be used instead of a code vector just like most visual tokenization works [7, 40]. And an additional network will be considered to generate condition codes instead of sampling weight collection for the case of a larger encoding space and conditional control generation. In addition, current sampling time schedule for diffusion models usually focus on low level of noise [12]. However, our method has the ability to reconstruct images with higher level of noise. Sampling method more suitable for our method is yet to be discovered. And further extension of our method to distillation or fine-tuning techniques is also highly anticipated.

6 Conclusion

In this paper, we show the degree of forward flow intersection will directly impact the generative performance of few-step sampling. We present a efficient plug-and-play method with a quite small additional training cost to reduce the average reconstruction loss, which is the first method that does not require trajectory relocation and additional regularization. Our approach preserves the critical properties of score-based models and is unique and complementary to other acceleration methods. We demonstrate that our approach improves the sample quality with a significantly reduced sampling budget.

References

1. Bengio, Y., Léonard, N., Courville, A.: Estimating or propagating gradients through stochastic neurons for conditional computation. arXiv preprint arXiv:1308.3432 (2013)
2. Berthelot, D., Autef, A., Lin, J., Yap, D.A., Zhai, S., Hu, S., Zheng, D., Talbot, W., Gu, E.: Tract: Denoising diffusion models with transitive closure time-distillation. arXiv preprint arXiv:2303.04248 (2023)
3. Cai, Z., Ravichandran, A., Maji, S., Fowlkes, C., Tu, Z., Soatto, S.: Exponential moving average normalization for self-supervised and semi-supervised learning. In: Proceedings of the IEEE/CVF Conference on Computer Vision and Pattern Recognition. pp. 194–203 (2021)
4. Choi, Y., Uh, Y., Yoo, J., Ha, J.W.: Stargan v2: Diverse image synthesis for multiple domains. In: Proceedings of the IEEE/CVF conference on computer vision and pattern recognition. pp. 8188–8197 (2020)
5. Chung, H., Kim, J., Mccann, M.T., Klasky, M.L., Ye, J.C.: Diffusion posterior sampling for general noisy inverse problems (2023)
6. Dockhorn, T., Vahdat, A., Kreis, K.: Genie: Higher-order denoising diffusion solvers (2022)
7. Esser, P., Rombach, R., Ommer, B.: Taming transformers for high-resolution image synthesis. In: Proceedings of the IEEE/CVF conference on computer vision and pattern recognition. pp. 12873–12883 (2021)
8. Ho, J., Jain, A., Abbeel, P.: Denoising diffusion probabilistic models. *Advances in Neural Information Processing Systems* **33**, 6840–6851 (2020)
9. Ho, J., Salimans, T.: Classifier-free diffusion guidance. arXiv preprint arXiv:2207.12598 (2022)
10. Ho, J., Salimans, T., Gritsenko, A., Chan, W., Norouzi, M., Fleet, D.J.: Video diffusion models (2022)
11. Hyvärinen, A., Dayan, P.: Estimation of non-normalized statistical models by score matching. *Journal of Machine Learning Research* **6**(4) (2005)
12. Karras, T., Aittala, M., Aila, T., Laine, S.: Elucidating the design space of diffusion-based generative models. *Advances in Neural Information Processing Systems* **35**, 26565–26577 (2022)
13. Karras, T., Laine, S., Aila, T.: A style-based generator architecture for generative adversarial networks. In: Proceedings of the IEEE/CVF conference on computer vision and pattern recognition. pp. 4401–4410 (2019)
14. Kingma, D., Salimans, T., Poole, B., Ho, J.: Variational diffusion models. *Advances in neural information processing systems* **34**, 21696–21707 (2021)
15. Kingma, D.P., Welling, M.: Auto-encoding variational bayes. arXiv preprint arXiv:1312.6114 (2013)
16. Kong, Z., Ping, W., Huang, J., Zhao, K., Catanzaro, B.: Diffwave: A versatile diffusion model for audio synthesis. arXiv preprint arXiv:2009.09761 (2020)
17. Krizhevsky, A., Hinton, G., et al.: Learning multiple layers of features from tiny images (2009)
18. Kwon, D., Fan, Y., Lee, K.: Score-based generative modeling secretly minimizes the wasserstein distance. *Advances in Neural Information Processing Systems* **35**, 20205–20217 (2022)
19. Lee, S., Kim, B., Ye, J.C.: Minimizing trajectory curvature of ode-based generative models. arXiv preprint arXiv:2301.12003 (2023)

20. Lipman, Y., Chen, R.T., Ben-Hamu, H., Nickel, M., Le, M.: Flow matching for generative modeling. arXiv preprint arXiv:2210.02747 (2022)
21. Liu, L., Ren, Y., Lin, Z., Zhao, Z.: Pseudo numerical methods for diffusion models on manifolds (2022)
22. Liu, X., Gong, C., et al.: Flow straight and fast: Learning to generate and transfer data with rectified flow. In: The Eleventh International Conference on Learning Representations (2022)
23. Lu, C., Zhou, Y., Bao, F., Chen, J., Li, C., Zhu, J.: Dpm-solver: A fast ode solver for diffusion probabilistic model sampling in around 10 steps. arXiv preprint arXiv:2206.00927 (2022)
24. Lu, C., Zhou, Y., Bao, F., Chen, J., Li, C., Zhu, J.: Dpm-solver++: Fast solver for guided sampling of diffusion probabilistic models (2023), <https://arxiv.org/abs/2211.01095>
25. Luhman, E., Luhman, T.: Knowledge distillation in iterative generative models for improved sampling speed. arXiv preprint arXiv:2101.02388 (2021)
26. Luo, W., Hu, T., Zhang, S., Sun, J., Li, Z., Zhang, Z.: Diff-instruct: A universal approach for transferring knowledge from pre-trained diffusion models. Advances in Neural Information Processing Systems **36** (2024)
27. Maoutsa, D., Reich, S., Opper, M.: Interacting particle solutions of fokker–planck equations through gradient–log–density estimation. Entropy **22**(8), 802 (Jul 2020). <https://doi.org/10.3390/e22080802>, <http://dx.doi.org/10.3390/e22080802>
28. Mentzer, F., Minnen, D., Agustsson, E., Tschannen, M.: Finite scalar quantization: Vq-vae made simple (2023)
29. Nichol, A.Q., Dhariwal, P.: Improved denoising diffusion probabilistic models. In: International Conference on Machine Learning. pp. 8162–8171. PMLR (2021)
30. Pooladian, A.A., Ben-Hamu, H., Domingo-Enrich, C., Amos, B., Lipman, Y., Chen, R.: Multisample flow matching: Straightening flows with minibatch couplings. arXiv preprint arXiv:2304.14772 (2023)
31. Poole, B., Jain, A., Barron, J.T., Mildenhall, B.: Dreamfusion: Text-to-3d using 2d diffusion. arXiv preprint arXiv:2209.14988 (2022)
32. Salimans, T., Ho, J.: Progressive distillation for fast sampling of diffusion models. arXiv preprint arXiv:2202.00512 (2022)
33. Salmona, A., de Bortoli, V., Delon, J., Desolneux, A.: Can push-forward generative models fit multimodal distributions? (2022)
34. Shao, S., Dai, X., Yin, S., Li, L., Chen, H., Hu, Y.: Catch-up distillation: You only need to train once for accelerating sampling (2023)
35. Song, J., Meng, C., Ermon, S.: Denoising diffusion implicit models. In: International Conference on Learning Representations (2020)
36. Song, Y., Dhariwal, P., Chen, M., Sutskever, I.: Consistency models. arXiv preprint arXiv:2303.01469 (2023)
37. Song, Y., Ermon, S.: Generative modeling by estimating gradients of the data distribution. Advances in neural information processing systems **32** (2019)
38. Song, Y., Sohl-Dickstein, J., Kingma, D.P., Kumar, A., Ermon, S., Poole, B.: Score-based generative modeling through stochastic differential equations. arXiv preprint arXiv:2011.13456 (2020)
39. Vahdat, A., Kreis, K., Kautz, J.: Score-based generative modeling in latent space. Advances in Neural Information Processing Systems **34**, 11287–11302 (2021)
40. Van Den Oord, A., Vinyals, O., et al.: Neural discrete representation learning. Advances in neural information processing systems **30** (2017)
41. Vincent, P.: A connection between score matching and denoising autoencoders. Neural computation **23**(7), 1661–1674 (2011)

42. Xue, S., Yi, M., Luo, W., Zhang, S., Sun, J., Li, Z., Ma, Z.M.: Sa-solver: Stochastic adams solver for fast sampling of diffusion models. *Advances in Neural Information Processing Systems* **36** (2024)
43. Yin, T., Gharbi, M., Zhang, R., Shechtman, E., Durand, F., Freeman, W.T., Park, T.: One-step diffusion with distribution matching distillation. *arXiv preprint arXiv:2311.18828* (2023)
44. Zhang, Q., Chen, Y.: Fast sampling of diffusion models with exponential integrator. *arXiv preprint arXiv:2204.13902* (2022)
45. Zhao, W., Bai, L., Rao, Y., Zhou, J., Lu, J.: Unipc: A unified predictor-corrector framework for fast sampling of diffusion models. *Advances in Neural Information Processing Systems* **36** (2024)
46. Zheng, K., Lu, C., Chen, J., Zhu, J.: Dpm-solver-v3: Improved diffusion ode solver with empirical model statistics (2023)
47. Zhou, Z., Chen, D., Wang, C., Chen, C.: Fast ode-based sampling for diffusion models in around 5 steps (2023)